

Review

Layered Perovskites $\text{BaLn}_n\text{In}_n\text{O}_{3n+1}$ ($n = 1, 2$) for Electrochemical Applications: A Mini Review

Nataliia Tarasova ^{1,2} 

¹ The Institute of High Temperature Electrochemistry of the Ural Branch of the Russian Academy of Sciences, 620066 Yekaterinburg, Russia; natalia.tarasova@urfu.ru

² Institute of Hydrogen Energy, Ural Federal University, 620075 Yekaterinburg, Russia

Abstract: Modern humanity is facing many challenges, such as declining reserves of fossil energy resources and their increasing prices, climate change and an increase in the number of respiratory diseases including COVID-19. This causes an urgent need to create advanced energy materials and technologies to support the sustainable development of renewable energy systems including hydrogen energy. Layered perovskites have many attractions due to their physical and chemical properties. The structure of such compounds contains perovskite layers divided by layers with different frameworks, which provide their properties' features. Proton-conduction layered perovskites open up a novel structural class of protonic conductors, potentially suitable for application in such hydrogen energy devices as protonic ceramic electrolysis cells and protonic ceramic fuel cells. In this mini review, the special features of proton transport in the novel class of proton conductors $\text{BaLn}_n\text{In}_n\text{O}_{3n+1}$ ($n = 1, 2$) with a layered perovskite structure are observed and general regularities are discussed.

Keywords: Ruddlesden–Popper structure; oxygen-ion conductivity; proton conductivity; proton-conducting solid oxide fuel cells



Citation: Tarasova, N. Layered Perovskites $\text{BaLn}_n\text{In}_n\text{O}_{3n+1}$ ($n = 1, 2$) for Electrochemical Applications: A Mini Review. *Membranes* **2023**, *13*, 34. <https://doi.org/10.3390/membranes13010034>

Academic Editors: Vladislav A. Sadykov, Christos Argirusis, Vladislav V. Kharton and Denis Osinkin

Received: 5 December 2022

Revised: 22 December 2022

Accepted: 23 December 2022

Published: 28 December 2022



Copyright: © 2022 by the author. Licensee MDPI, Basel, Switzerland. This article is an open access article distributed under the terms and conditions of the Creative Commons Attribution (CC BY) license (<https://creativecommons.org/licenses/by/4.0/>).

1. Introduction

Modern humanity is facing many challenges, such as declining reserves of fossil energy resources and their increasing prices [1–4], climate change [5–8] and an increase in the number of respiratory diseases including COVID-19 [9,10]. This causes an urgent need to create advanced energy materials and technologies for supporting the sustainable development of renewable energy systems [11–15]. Hydrogen energy, due to eco-friendliness and high efficiency, has a high priority among other renewable energy systems [16–22]. The joining of forces in the fields of inorganic materials science and engineering for energy production has allowed the creation of such devices for hydrogen production as protonic ceramic electrolysis cells and devices for using hydrogen as a fuel for protonic ceramic fuel cells [23–34]. Among other materials, such devices need proton-conducting materials with a high level of proton conductivity and high resistance to carbon dioxide and water vapors [35].

The classic materials investigated as protonic conductors for over forty years such as barium cerates and zirconates have a perovskite structure [36–40]. The realization of protonic conductivity in such types of materials is due to the dissociative intercalation of water molecules into a crystal lattice of complex oxides and subsequent proton transport. Consequently, an increase in proton concentration and mobility should lead to an increase in protonic conductivity in the general case:

$$\sigma_i = z_i \cdot e \cdot c_i \cdot \mu_i, \quad (1)$$

where σ is the electrical conductivity; z is the charge of current carriers; c and μ are their corresponding concentration and mobility. The possibility of water uptake for the complex oxides with the perovskite structure ABO_3 (Figure 1a) is due to the creation of oxygen vacancies in the structure by the acceptor doping $AB_{1-x}M_xO_{3-\delta}$:



where $V_o^{\bullet\bullet}$ is the oxygen vacancy; O_o^{\times} is the oxygen atom in the regular position; $(OH)_o^{\bullet}$ is the hydroxyl group in the oxygen sublattice. In this case, the oxygen vacancy concentration is strongly dependent on the acceptor dopant concentration $[V_o^{\bullet\bullet}] = \frac{1}{2}[M'_B]$ and it does not exceed 0.15–0.20 mol water per complex oxide formula unit.

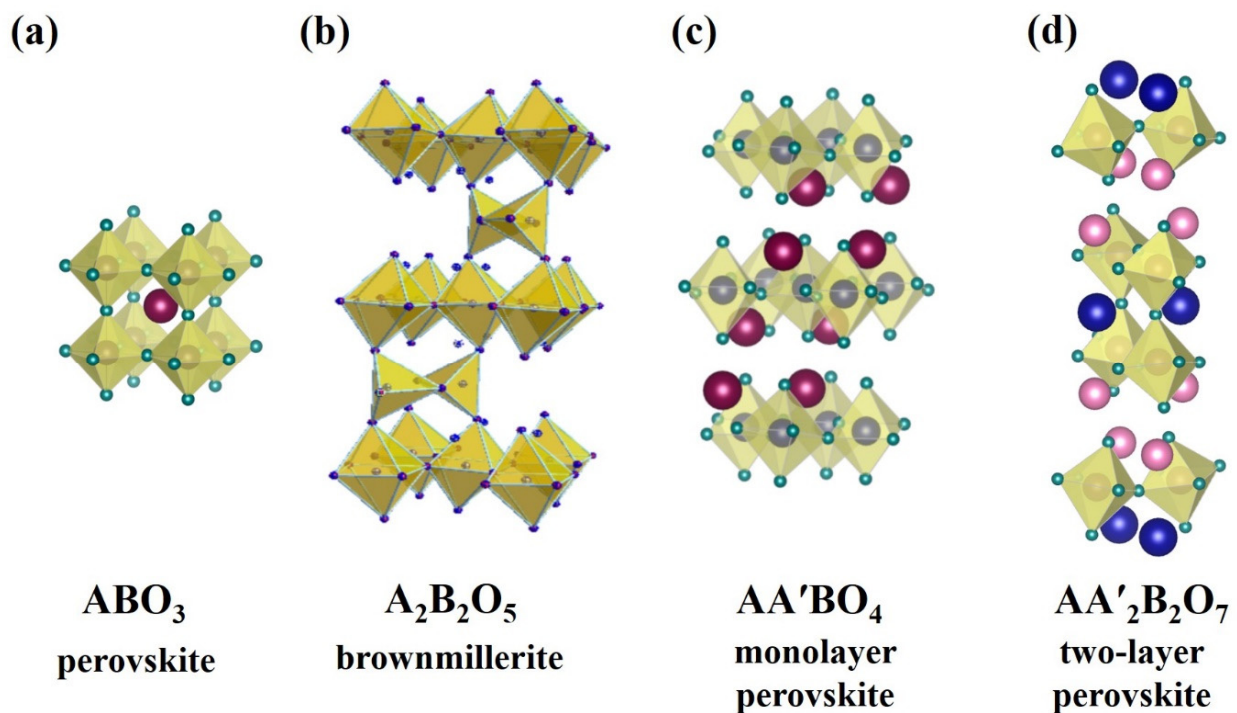


Figure 1. Crystal structures of perovskite (a), brownmillerite (b), monolayer (c) and two-layer (d) perovskites.

The increase in the oxygen vacancies in the structure can be obtained not only by the modification of the matrix complex oxide structure but also by the principal change in the structural class of material. The acceptor-doped perovskites have an impure oxygen disorder, but the perovskite-related materials with their own structural oxygen disorders such as $A_4B_2B'_2O_{11}$ (for example $Ba_4Ca_2Nb_2O_{11}$ [41]) and $A_2B_2O_5$ (Figure 1b) (for example $Ba_2In_2O_5$ [42]) are known. The maximal water uptake is achieved for materials with the brownmillerite structure $A_2B_2O_5 \equiv ABO_{2.5}$ and it is 0.5 mol water per perovskite formula unit:



where V_o^{\times} is the structural oxygen vacancy; O_o^{\times} is the oxygen atom in the regular position; $(OH)_o^{\bullet}$ is the hydroxyl group in the oxygen sublattice; $O_i^{\prime\prime}$ is the oxygen atom in the interstitial position. Further, overcoming the limitation of the proton concentration in the complex oxide structure needs the next materials search among other perovskite-related structures. In the last decade, layered perovskites have been investigated as prospective materials for use in such electrochemical devices as solid oxide fuel cells (Figure 2), mostly

however as electrode materials. In this paper, the details of proton transport in the novel class of proton conductors $BaLn_nIn_nO_{3n+1}$ ($n = 1, 2$) with a layered perovskite structure are observed and general regularities are discussed.

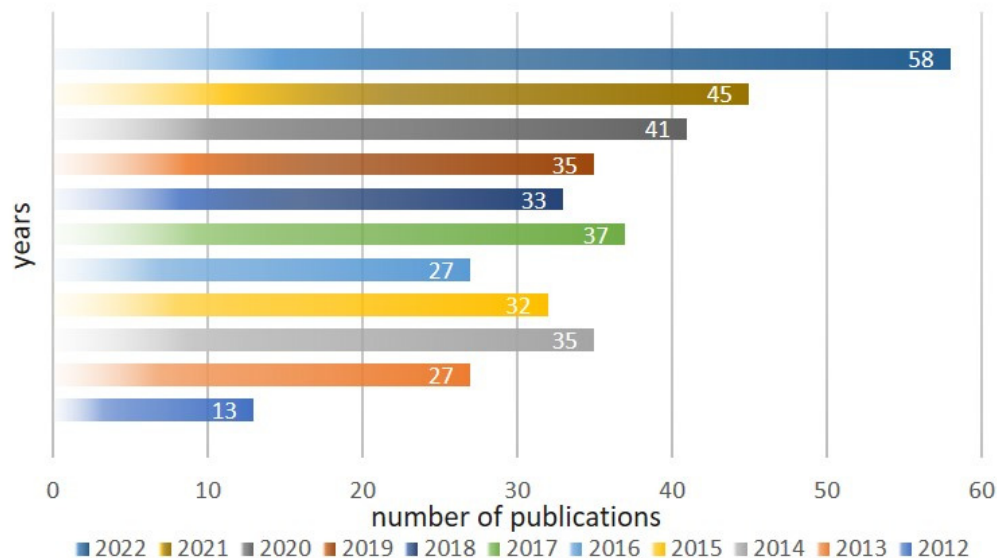


Figure 2. The progress of recent investigations into layered perovskites as prospective materials for solid oxide fuel cells.

2. Structural Features of Layered Perovskite-Related Materials

In general, layered perovskites can be described as compounds containing perovskite layers divided by layers with different frameworks that provide their property features. Layered perovskites can be classified as Ruddlesden–Popper, Dion–Jacobson and Aurivillius structures. The last two are mostly represented by materials with photocatalytic [43–53], ferroelectric [54–58] and luminescent [59–63] properties. In this paper, we focused on the proton-conducting layered perovskites with a Ruddlesden–Popper structure, which represent a large novel class of proton-conducting materials. They can be described by the general formula $A_{n+1}B_nO_{3n+1}$, in which rock salt layers AO and perovskite blocks $(ABO_3)_n$ are contained. The alternation of rock salt layers and perovskite blocks was described for the first time by S.N. Ruddlesden and P. Popper with the examples of the Sr_2TiO_4 [64] and $Sr_2Ti_2O_7$ [65] compounds about sixty-five years ago.

Some of crystal chemical criteria for the existence of layered Ruddlesden–Popper structures such as cation size ratio $\frac{\bar{R}_A}{\bar{R}_B}$ and bond ionicity I_{AO} , where

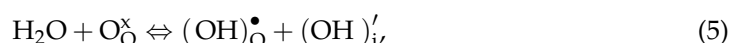
$$I_{AO} = \frac{i_{AO}}{i_{AO} + i_{BO}} \tag{4}$$

are highlighted [66–68]. The monolayer ($n = 1$) $AA'BO_4$ compositions should have $\frac{\bar{R}_A}{\bar{R}_B}$ in the range 1.473–2.78, and I_{AO} between 0.523 and 0.628. The two-layer ($n = 2$) $AA'_2B_2O_7$ compositions are characterized by a cation size ratio $\frac{\bar{R}_A}{\bar{R}_B}$ 1.606–2.262 and bond ionicity I_{AO} 0.519–0.624. In addition, the compositions must have tetragonal symmetry I_4/mmm when the cation size ratio is higher than 1.75 and 1.87 for monolayer and two-layer structures, correspondingly.

Many monolayer $AA'BO_4$ (Figure 1c) compositions including $BaLaInO_4$ have the coordination formula $A^{IX}A'^{IX}B^{VI}O_4^{VI}$ [69]. However, the distortion of the crystal lattice leads to the possibility of other metal coordination numbers. For example, the $BaNdInO_4$ composition is characterized by monoclinic symmetry and it has an $A^{XI}A'^{VII}B^{VI}O_4^{VI}$ coordination formula [70]. The two-layer perovskites (Figure 1d) have an $A^{XII}A'_2B_2^{VI}O_7^{VI}$ coordination formula, and perovskite blocks consist of tilted $[BO_6]$ octahedra [68]. This

structure is characterized by the ordered arrangement of A- and A'-cations, which can be represented as [AO₁₂] and [A'O₉]. In the other words, the A-cations are located between [BO₆] octahedra in the perovskite blocks, and the A'-cations are located in the rock salt layers. The ionic radius of the A'-cations is less than the A-cations, i.e., those kinds of atoms enter the inter-block space, whose ionic radius is lower. The decrease in the ionic radius of the rare-earth metal Ln for the layered perovskites A^{II}Ln_nB^{III}_nO_{3n+1} leads to the decrease in the space between perovskite blocks, i.e., to the decrease in the Ln–O2 bond and to the increase in [LnO₉] polyhedra deformation. This is the reason for the increase in the destabilization of the layered perovskite structure and its approaching a classical perovskite structure.

The presence in the structure of layered perovskites the atoms of which can increase their coordination numbers (A^{IX} → A^{XII}, for example) leads to the possibility of water uptake without the existence of oxygen vacancies (Figure 3). This process can be described as:



where (OH)_o[•] is the hydroxyl group in the regular oxygen position; (OH)_i' is the hydroxyl group located in the salt rock space. In the other words, the incorporated hydroxyl groups are placed into the salt block space. Consequently, the size of the salt block should play a significant role in the hydration properties of layered perovskites.

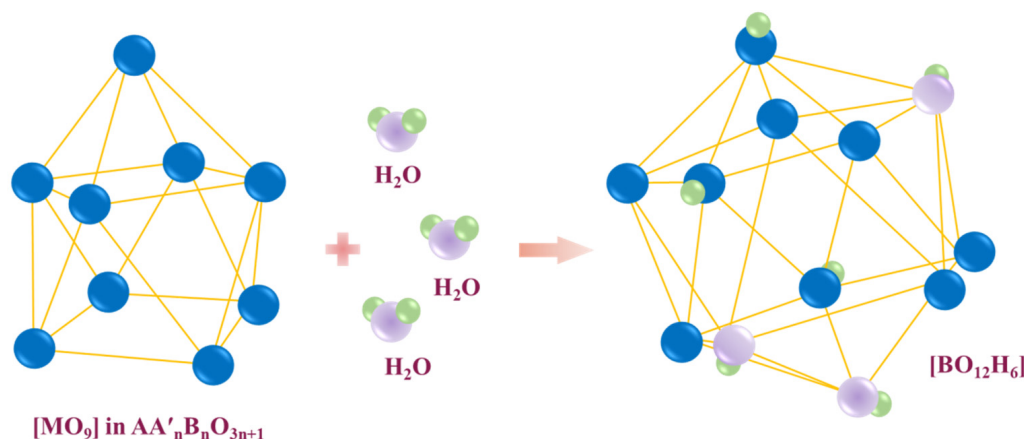


Figure 3. The schematic representation of the transformation of polyhedra [MO₉] to [MO₁₂] upon hydration.

3. Oxygen-Ionic Transport in Layered Perovskite-Related Materials

The oxygen-ionic transport through the crystal lattice of layered perovskites can be described as the migration of oxygen point defects existing in the crystal due to anion Frenkel disorder:

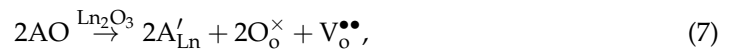


where O_o[×] is the oxygen atom in the regular position; V_o^{••} is the oxygen vacancy; O_i^{''} is the oxygen atom in the interstitial position. Doping (acceptor and donor) leads to changes in the oxygen stoichiometry, and hypostoichiometry and hyperstoichiometry are the result. Consequently, three possible oxygen migration mechanisms: (i) the direct interstitial mechanism, (ii) the interstitialcy mechanism and (iii) the vacancy mechanism can be considered [71]. The oxygen migration in monolayer perovskites where all elements have stable oxidation states is described by Yang et al. [72] and by Fujii et al. [73] for acceptor-doped compositions based on BaNdInO₄. Both are proposed 2D oxygen ion diffusion mechanisms within rock salt layers. The mechanism of oxygen-ionic transport for the two-layer perovskite BaLn₂In₂O₇ approved by calculation methods such as molecular dynamic simulation is not provided yet. However, we can suppose that ionic conductivity values must depend on the crystal structure features of layered compositions. The ratios of

salt layers and perovskite blocks are 1:1 and 1:2 for monolayer and two-layer perovskites, correspondingly. Consequently, the ionic conductivity for two-layer perovskites must be lower in comparison with the conductivity for monolayer perovskites in the case of the realization of the 2D oxygen ion diffusion mechanisms for both. Oppositely, conductivity for the $\text{BaLn}_2\text{In}_2\text{O}_7$ composition will be higher than for BaLnInO_4 if the 3D transport mechanism is realized for the first.

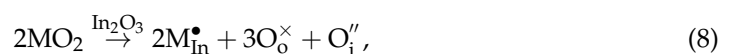
Figure 4 represents the temperature dependencies of the electrical conductivity values obtained under dry air for the monolayers BaLaInO_4 [74] and BaNdInO_4 [70,71] and the two-layer $\text{BaLa}_2\text{In}_2\text{O}_7$ [74] and $\text{BaNd}_2\text{In}_2\text{O}_7$ [75] compositions. All of these samples were obtained by the solid-state method. The qualitative and quantitative compositions of the samples were confirmed by various methods such as XRD, SEM, EDS, EDX, etc. As can be seen, conductivity increases in the rows BaLaInO_4 - BaNdInO_4 and $\text{BaLa}_2\text{In}_2\text{O}_7$ - $\text{BaNd}_2\text{In}_2\text{O}_7$; i.e., Nd-containing compositions are more conductive than La-containing ones despite the number of n in the layered $\text{BaLn}_n\text{In}_n\text{O}_{3n+1}$ structure. At the same time, two-layer compositions are more conductive than monolayer compounds. That is, the assumption about the 3D oxygen ion diffusion mechanism for two-layer perovskites $\text{BaLn}_2\text{In}_2\text{O}_7$ is confirmed.

The acceptor doping of the layered perovskites $\text{BaLn}_n\text{In}_n\text{O}_{3n+1}$ can be described as:



where A'_{Ln} is the acceptor dopant in the sublattice of the rare-earth metal Ln; O_o^\times is the oxygen atom in the regular position; $\text{V}_\text{o}^{\bullet\bullet}$ is the oxygen vacancy. The appearance of oxygen vacancies in the crystal lattice of layered perovskites leads to the increase in conductivity values for both the monolayer BaLnInO_4 and two-layer $\text{BaLa}_2\text{In}_2\text{O}_7$ compositions. However, some features can be highlighted. Firstly, the increase in the conductivity values for the monolayer BaLaInO_4 [76–83] and BaNdInO_4 [70,72,73,84–86] compositions is more significant than for the two-layer $\text{BaLa}_2\text{In}_2\text{O}_7$ [74,87–90] and $\text{BaNd}_2\text{In}_2\text{O}_7$ [75,91] compositions (~1.5 vs. ~1. order of magnitude). Secondly, both the monolayer BaLnInO_4 and two-layer $\text{BaLn}_2\text{In}_2\text{O}_7$ compositions have different conductivity values with the same acceptor dopant concentration. Thirdly, the conductivity changes non-linearly with the increase in oxygen vacancy concentration.

The donor doping of the layered perovskite $\text{BaLn}_n\text{In}_n\text{O}_{3n+1}$ can be described as:



where $\text{M}^\bullet_{\text{In}}$ is the donor dopant in the indium sublattice; O''_{i} is the oxygen atom in the interstitial position. As opposed to acceptor doping, donor doping can be realized only for the monolayer BaLnInO_4 composition. The only mention of donor-doped two-layered composition was for $\text{BaLa}_2\text{In}_{0.9}\text{Ti}_{0.1}\text{O}_{7.05}$; however, the conductivity values for it were lower than for the undoped $\text{BaLa}_2\text{In}_2\text{O}_7$ composition [78]. Consequently, it can be summarized that the crystal lattice of the two-layer $\text{BaLn}_2\text{In}_2\text{O}_7$ perovskites is less tolerant to the presence of “additional” interstitial oxygen in comparison with the monolayer BaLnInO_4 perovskites. The possibility of isovalent doping was proved for the monolayer and two-layer La-containing composition. The compositions with the doping of the La-sublattice $\text{BaLa}_{0.9}\text{Gd}_{0.1}\text{InO}_4$ [81], $\text{BaLa}_{0.9}\text{Nd}_{0.1}\text{InO}_4$ [82], $\text{BaLa}_{2-x}\text{Gd}_x\text{In}_2\text{O}_7$ $0 \leq x \leq 0.15$ [90] and In-sublattice $\text{BaLaIn}_{0.9}\text{Sc}_{0.1}\text{O}_4$ [79], $\text{BaLaIn}_{1-x}\text{Y}_x\text{O}_4$ ($0 \leq x \leq 0.5$) [80] were obtained and investigated.

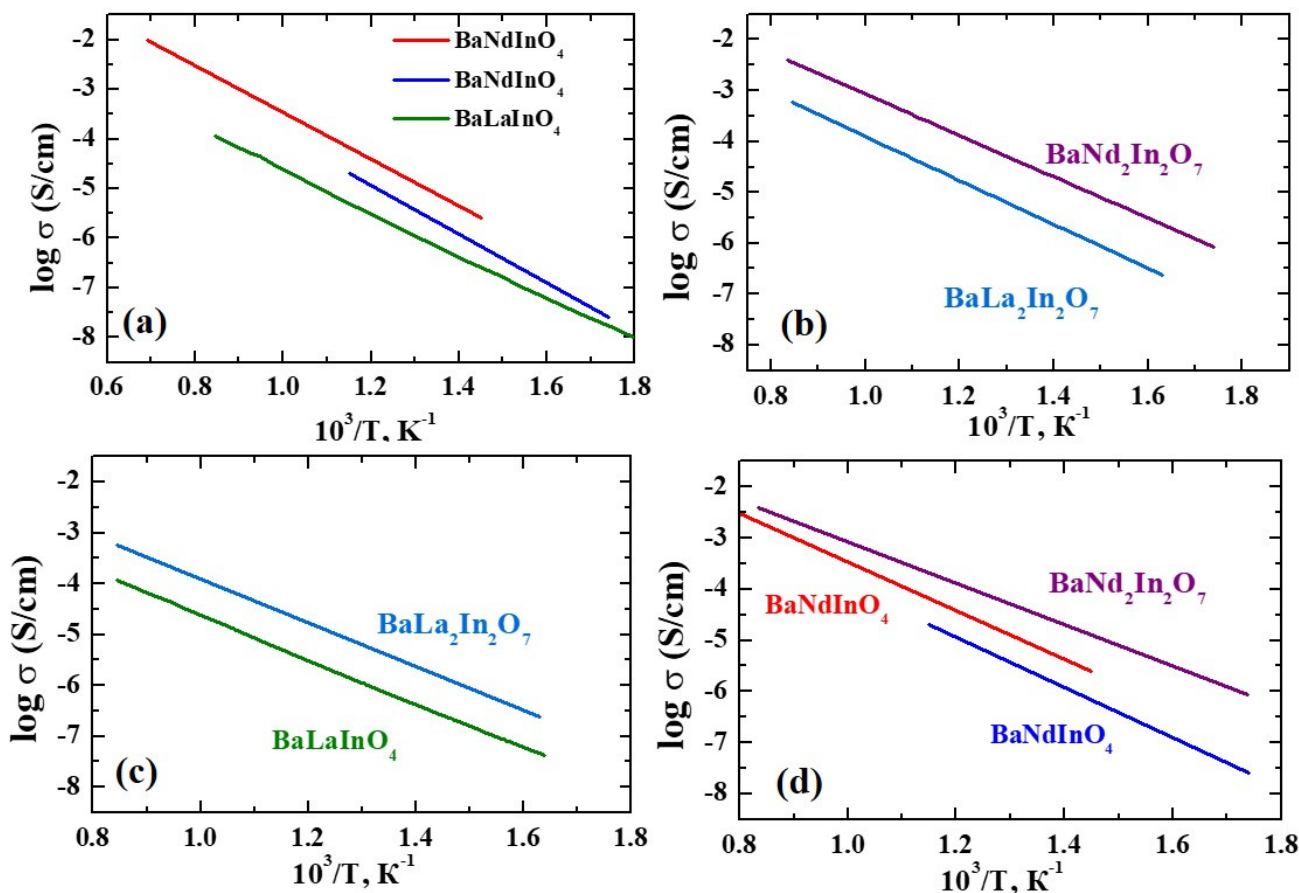


Figure 4. The temperature dependencies of electrical conductivity values obtained under dry air for monolayer BaLaInO₄ [74], BaNdInO₄ [70,71] compositions (a), two-layer BaLa₂In₂O₇ [74] and BaNd₂In₂O₇ [75] compositions (b), La-containing BaLaInO₄ [74] and BaLa₂In₂O₇ [74] compositions (c), Nd-containing BaNdInO₄ [70,71] and BaNd₂In₂O₇ [75] compositions (d).

The correlation between changes in the structural characteristics (lattice parameters, unit cell volumes) and conductivity values for doped compositions based on BaLaInO₄ and BaLa₂In₂O₇ is presented in Figure 5. The increase in the unit cell volume for monolayer compositions is due to the increase in the *a* lattice parameter, which indicates the increase in the distance between perovskite blocks. In general, this increase correlates well with the increase in electrical conductivity values upon doping. It allows us to say that the geometric factor has a significant effect on the change in electrical conductivity. This is also a key factor in understanding why related compositions have different conductivity at the same concentration of oxygen vacancies. It should be noted that the reasons for the increase in lattice parameters are different for each type of doping. The introduction of acceptor dopants with bigger ionic radii (Sr/Ba → La), the appearance of “additional” interstitial oxygen during donor doping and the appearance of the additional repulsion effects of the different nature ions in one sublattice during isovalent doping can be named as the more significant reasons for the increase in the *a* lattice parameter.

For two-layer perovskites based on BaLa₂In₂O₇, the clearer correlation is between the *c* lattice parameter, which indicates the increase in the distance between perovskite blocks for this type of crystal structure, and conductivity values. As it was for monolayer compositions, the increase in the distance between perovskite blocks leads to the increase in the conductivity values. However, this increase is smaller, which can be explained by different conduction mechanisms for each type of layered structure.

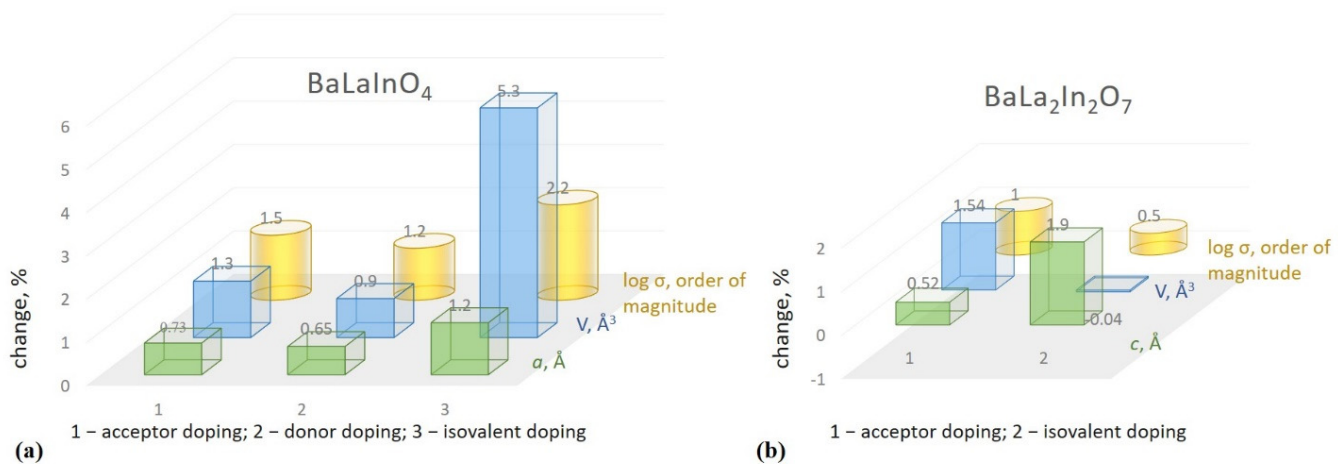


Figure 5. The changes in the lattice parameters, unit cell volumes and oxygen-ionic conductivity values for doped compositions based on monolayer BaLaInO₄ (a) and two-layer BaLa₂In₂O₇ perovskites (b).

Despite the increase in distance between perovskite blocks during heterovalent (donor and acceptor) doping, conductivity values increase at the “small” dopant concentrations (i.e., at “small” oxygen point defect ($V_o^{\bullet\bullet}$ or O_i'') concentrations) and decrease at the “big” concentrations. The most probable reason is the formation of clusters with lower mobility and a decrease in the concentration of mobile oxygen defects. The defect association can describe the acceptor type of doping as:



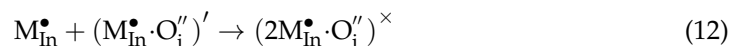
or



and for the donor type of doping as



or



It is clear that both factors, the increase in the lattice parameters (geometric factor) and the increase in the oxygen defects concentration (concentration factor), affect the electrical conductivity value simultaneously. Consequently, the exclusion of one of these factors can help determine the most significant cause of changes in the electrical conductivity values. Both heterovalent doping and isovalent doping lead to an increase in the lattice parameters, but the oxygen concentration does not change.

Figure 6 represents the concentration dependencies of the oxygen-ionic conductivities for heterovalent-doped BaLa_{1-x}Ba_xInO_{4-0.5x} [76], BaLaIn_{1-x}Ti_xO_{4+0.5x} [78], BaLa_{2-x}Ba_xIn₂O_{7-x} [89] and isovalent-doped BaLaIn_{1-x}Y_xO₄ [80], BaLa_{2-x}Gd_xIn₂O₇ [91] compositions. As can be seen, isovalent doping allows the obtaining of more conductive compositions at the same dopant concentration for monolayer perovskites based on BaLaBaInO₄. Conversely, acceptor doping is a more suitable way to increase the conductivity values of two-layered perovskites compared with isovalent doping. The crystal lattice of monolayer BaLaInO₄ perovskites is more flexible than two-layer BaLa₂In₂O₇ perovskites, which allows for a more significant increase in the distance between perovskite blocks and in the conductivity values. However, the decrease in the conductivity values at a “big” acceptor dopant concentration is more valuable for monolayer BaLa_{1-x}Ba_xInO_{4-0.5x} perovskites compared with two-layer BaLa_{2-x}Ba_xIn₂O_{7-x}. We can suppose that the reason for this difference is the change in the ratio of perovskite blocks and salt layers and in the mechanism of oxygen transport.

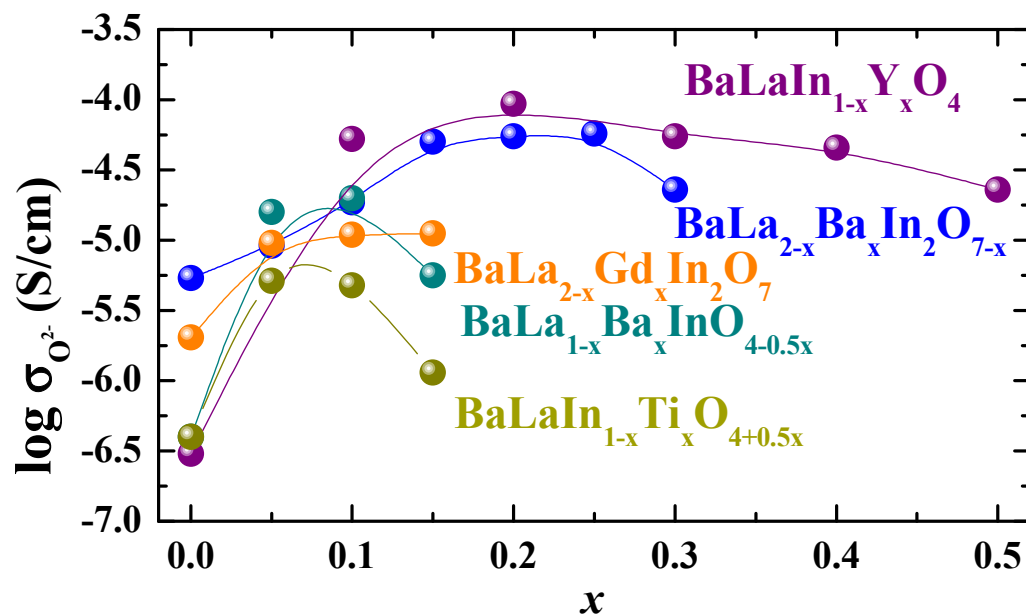


Figure 6. The concentration dependencies of oxygen-ionic conductivities for heterovalent-doped $\text{BaLa}_{1-x}\text{Ba}_x\text{InO}_{4-0.5x}$ [76], $\text{BaLaIn}_{1-x}\text{Ti}_x\text{O}_{4+0.5x}$ [78], $\text{BaLa}_{2-x}\text{Ba}_x\text{In}_2\text{O}_{7-x}$ [89] and isovalent-doped $\text{BaLaIn}_{1-x}\text{Y}_x\text{O}_4$ [80], $\text{BaLa}_{2-x}\text{Gd}_x\text{In}_2\text{O}_7$ [91] compositions at 500 °C.

4. Proton Transport in Layered Perovskite-Related Materials

Protonic conductivity directly depends on the proton concentration in the structure (Equation (1)), and the possibility of water uptake for layered perovskites is very important. The possibility for water intercalation for undoped and doped layered BaLaInO_4 perovskites was proved, and the absence of correlation between oxygen vacancy concentration and water uptake was shown [77]. Figure 7a represents the dependency of water uptake vs. unit cell volume for monolayer perovskites. As we can see, the water uptake for doped perovskites based on BaLaInO_4 is much higher than for classical ABO_3 perovskites (up to ~2 mol water per complex oxide formula unit). In addition, the water uptake for isovalent-doped compositions is higher in comparison with isovalent-doped compositions. The possible reason is the absence of “additional” oxygen point defects ($\text{V}_\text{O}^{\bullet\bullet}$ or O_I'') in the salt layer space, which can make the dissociative intercalation of water molecules into the crystal lattice difficult.

The dependency of water uptake vs. unit cell volume for two-layer perovskites is presented in the Figure 7b. Contrary to monolayer perovskites, the changes in the unit cell volume do not significantly affect the amount of water uptake. It slightly increases with the increase in oxygen concentration, but it does not reach the maximum possible values equal to the concentration of vacancies. In general, the water uptake for all undoped and doped two-layer perovskites based on $\text{BaLn}_2\text{In}_2\text{O}_7$ is about 0.10–0.22 mol per complex oxide formula unit [87], which is comparable with the values for acceptor-doped classic perovskites.

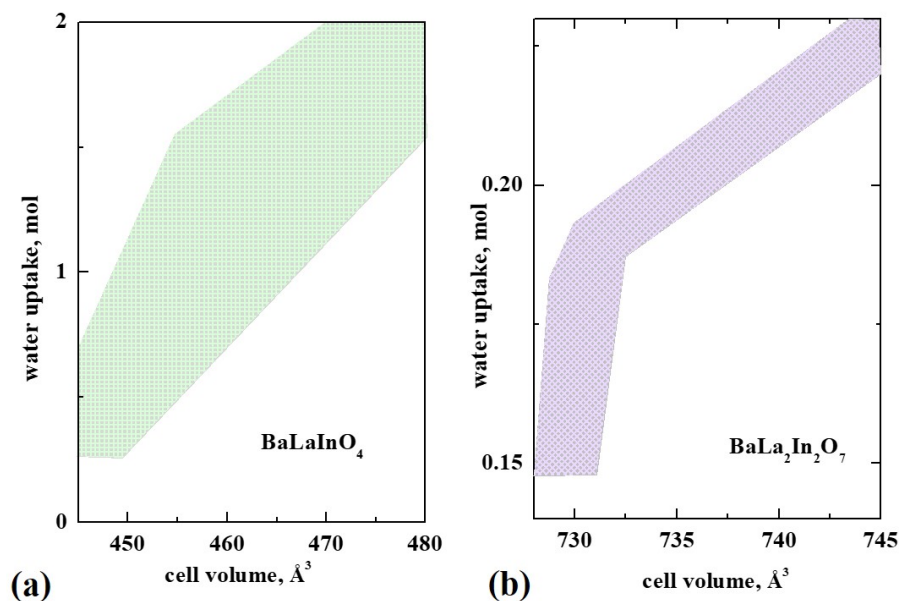


Figure 7. The dependencies of water uptake for doped compositions based on BaLaInO₄ monolayer (a) and two-layer BaLa₂In₂O₇ (b) perovskites.

The concentration dependencies of the proton conductivity values for monolayer and two-layer compositions are presented in Figure 8. As can be seen, the general regularities of protonic conductivity are similar to the regularities of oxygen-ionic conductivity (Figure 6). The decrease in the proton conductivity at a “big” dopant concentration is observed for heterovalent-doped monolayer perovskites based on BaLaInO₄. The cluster formation can be named as the reason for this decrease and it can be expressed by the following equations:

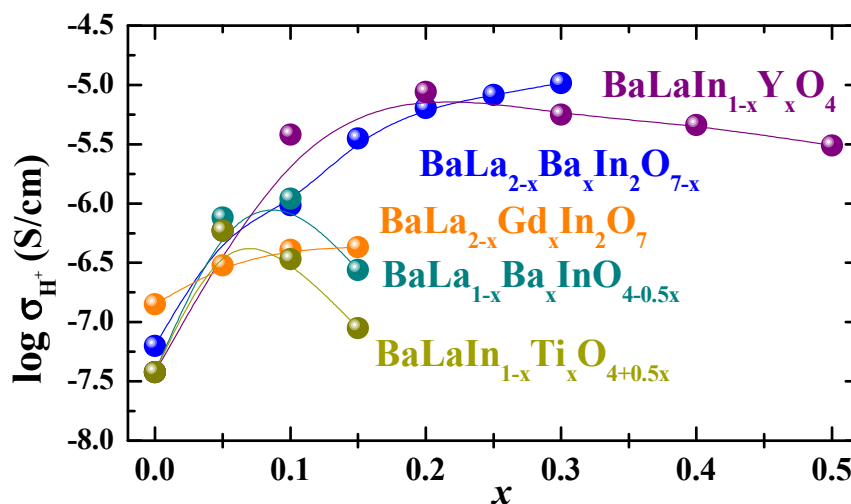
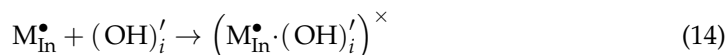
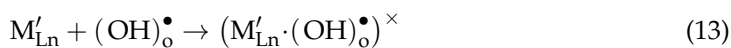


Figure 8. The concentration dependencies of protonic conductivities for heterovalent-doped BaLa_{1-x}Ba_xInO_{4+0.5x} [76], BaLaIn_{1-x}Ti_xO_{4+0.5x} [78], BaLa_{2-x}Ba_xIn₂O_{7-x} [86] and isovalent-doped BaLaIn_{1-x}Y_xO₄ [80], BaLa_{2-x}Gd_xIn₂O₇ [90] compositions at 300 °C.

The greatest increase in conductivity is achieved by isovalent doping for monolayer compositions and by acceptor doping for two-layer compositions. The comparison of the protonic conductivity values of layered perovskites BaLn_nIn_nO_{3n+1} (n = 1, 2) is presented

in Table 1. The conductivity values for most conductive monolayer $\text{BaLaIn}_{1-x}\text{Y}_x\text{O}_4$ and two-layer $\text{BaLa}_{2-x}\text{Ba}_x\text{In}_2\text{O}_{7-x}$ compositions are comparable. This allows us to say that a significant decrease (about one order of magnitude) in the proton concentration for two-layer perovskites compared to monolayer perovskites is compensated for by the increase in their mobility. Obviously, this increase is due to the increase in oxygen-ion mobility since the transfer of protons is carried out by moving along oxygen ions. We can suggest that the inclusion of perovskite blocks in the crystal lattice (two-layer perovskites) and the creation of oxygen vacancies into them (acceptor doping) change the transport mechanism from 2D to 3D and significantly increase the ionic conductivity values. In general, an increase in the number of perovskite stacks in the blocks of the layered structure leads to an increase in the ionic conductivity values of the layered perovskites $\text{BaLn}_n\text{In}_n\text{O}_{3n+1}$ ($n = 1, 2$).

Table 1. The comparison of the protonic conductivity values of layered perovskites $\text{BaLn}_n\text{In}_n\text{O}_{3n+1}$ ($n = 1, 2$).

Composition	Values of Protonic Conductivity at 450 °C, S/cm	Ref.
BaLaInO_4	4×10^{-7}	[83]
$\text{Ba}_{1.1}\text{La}_{0.9}\text{InO}_{3.95}$	0.8×10^{-5}	[83]
$\text{BaLa}_{0.9}\text{Sr}_{0.1}\text{InO}_{3.95}$	1.4×10^{-5}	[83]
$\text{BaLa}_{0.9}\text{Ca}_{0.1}\text{InO}_{3.95}$	1.9×10^{-5}	[83]
$\text{BaLaIn}_{0.9}\text{Ti}_{0.1}\text{O}_{4.05}$	0.2×10^{-5}	[78]
$\text{BaLaIn}_{0.9}\text{Zr}_{0.1}\text{O}_{4.05}$	0.2×10^{-5}	[78]
$\text{BaLa}_{0.9}\text{Nd}_{0.1}\text{InO}_4$	1.1×10^{-5}	[82]
$\text{BaLa}_{0.9}\text{Gd}_{0.1}\text{InO}_4$	1.0×10^{-5}	[81]
$\text{BaLaIn}_{0.1}\text{Y}_{0.9}\text{O}_4$	3.3×10^{-5}	[80]
$\text{BaLaIn}_{0.1}\text{Sc}_{0.9}\text{O}_4$	1.2×10^{-5}	[79]
$\text{BaLa}_2\text{In}_2\text{O}_7$	1.7×10^{-6}	[75]
$\text{BaLa}_{0.9}\text{Ca}_{0.1}\text{InO}_{3.95}$	2.3×10^{-6}	[74]
$\text{Ba}_{1.05}\text{La}_{1.95}\text{In}_2\text{O}_{6.975}$	5.4×10^{-6}	[87]
$\text{Ba}_{1.1}\text{La}_{1.9}\text{In}_2\text{O}_{6.95}$	10×10^{-6}	[87]
$\text{Ba}_{1.2}\text{La}_{1.8}\text{In}_2\text{O}_{6.9}$	63×10^{-6}	[87]
$\text{Ba}_{1.25}\text{La}_{1.75}\text{In}_2\text{O}_{6.875}$	64×10^{-6}	[87]
$\text{BaLa}_{1.9}\text{Sr}_{0.1}\text{In}_2\text{O}_{6.95}$	9.4×10^{-6}	[87]
$\text{BaLa}_{1.85}\text{Sr}_{0.15}\text{In}_2\text{O}_{6.925}$	14×10^{-6}	[87]
$\text{BaLa}_{1.8}\text{Sr}_{0.2}\text{In}_2\text{O}_{6.9}$	17×10^{-6}	[87]
$\text{BaLa}_{1.95}\text{Gd}_{0.05}\text{In}_2\text{O}_7$	1.8×10^{-6}	[90]
$\text{BaLa}_{1.9}\text{Gd}_{0.1}\text{In}_2\text{O}_7$	2.3×10^{-6}	[90]
$\text{BaLa}_{1.85}\text{Gd}_{0.15}\text{In}_2\text{O}_7$	2.7×10^{-6}	[90]

One of the next steps for using layered perovskites for electrochemical applications is the transition from material creation to manufacturing technology. In this regard, the problem of comparability between materials of different device components such as electrode and electrolyte materials becomes very important. We believe that the investigation of stacks where both electrode and electrolyte materials have a layered structure will happen in the near future.

5. Conclusions

In this paper, the specifics of proton transport in the novel class of proton conductors $\text{BaLn}_n\text{In}_n\text{O}_{3n+1}$ ($n = 1, 2$) with a layered perovskite structure are observed and general regularities are discussed. The conductivity values are strongly dependent on the nature of the rare-earth metal Ln and of a number of perovskite n stacks in the structure. The Nd-containing compositions are more conductive than the La-containing ones at the same n . When the nature of the rare-earth metal does not change, two-layer perovskites have higher conductivity values in comparison with monolayer compounds. The crystal lattice of monolayer perovskites is more “flexible” and allows the performance of various types of doping such as acceptor, donor and isovalent doping, while donor doping is not suitable

for the two-layer perovskite structure. The water uptake for doped monolayer perovskites is much higher than for classical ABO_3 perovskites (up to ~ 2 mol water per complex oxide formula unit) and it is comparable (~ 0.2 mol water) for two-layer perovskites. The greatest increase in conductivity is achieved by isovalent doping for monolayer compositions and by acceptor doping for two-layer compositions. At the same time, the conductivity values for most conductive monolayer $BaLaIn_{1-x}Y_xO_4$ and two-layer $BaLa_{2-x}Ba_xIn_2O_{7-x}$ compositions are comparable.

We can conclude that the increase in the number of perovskite stacks in the blocks of the layered structure approaches the properties of the layered perovskite closer to classical perovskite. The ionic conductivity values of layered perovskites $BaLn_nIn_nO_{3n+1}$ ($n = 1, 2$) increase with increasing n , but the water uptake decreases. At the same time, layered perovskites are a prospective class due to their structural “flexibility”, ability to vary the concentration of protons and conductivity over a wide range (up to 2 orders of magnitude) during doping. The optimal combination of cations and doping method will allow the obtaining of novel high-conductive materials suitable for application as protonic electrolytes in different electrochemical devices, and the next materials search will be very relevant.

Funding: This research was supported by the Russian Science Foundation (grant no 22-79-10003).

Institutional Review Board Statement: Not applicable.

Data Availability Statement: Not applicable.

Conflicts of Interest: The authors declare no conflict of interest.

References

1. Malerba, D. Poverty-energy-emissions pathways: Recent trends and future sustainable development goals. *Int. J. Sustain. Energy Dev.* **2019**, *49*, 109–124. [[CrossRef](#)]
2. Buonomano, A.; Barone, G.; Forzano, C. Advanced energy technologies, methods, and policies to support the sustainable development of energy, water and environment systems. *Energy Rep.* **2022**, *8*, 4844–4853. [[CrossRef](#)]
3. Chu, S.; Majumdar, A. Opportunities and challenges for a sustainable energy future. *Nature* **2012**, *48*, 294–303. [[CrossRef](#)] [[PubMed](#)]
4. Østergaard, P.A.; Duic, N.; Noorollahi, Y.; Mikulcic, H.; Kalogirou, S. Sustainable development using renewable energy technology. *Renew. Energy* **2020**, *146*, 2430–2437. [[CrossRef](#)]
5. Olabi, A.G.; Abdelkareem, M.A. Renewable energy and climate change. *Renew. Sustain. Energy Rev.* **2022**, *158*, 112111. [[CrossRef](#)]
6. Corvalan, C.; Prats, E.V.; Sena, A.; Varangu, L.; Vinci, S. Towards climate resilient and environmentally sustainable health care facilities. *Int. J. Environ. Res. Public Health* **2020**, *17*, 8849. [[CrossRef](#)]
7. Watts, N.; Amann, M.; Arnell, N.; Montgomery, H.; Costello, A. The 2020 report of the Lancet countdown on health and climate change: Responding to converging crises. *Lancet* **2021**, *397*, 129–170. [[CrossRef](#)]
8. Kats, G.H. Slowing global warming and sustaining development: The promise of energy efficiency. *Energy Policy* **1990**, *18*, 25–33. [[CrossRef](#)]
9. Afroze, S.; Reza, M.S.; Cheok, Q.; Taweekun, J.; Azad, A.K. Solid oxide fuel cell (SOFC); A new approach of energy generation during the pandemic COVID-19. *Int. J. Integr. Eng.* **2020**, *12*, 245–256. [[CrossRef](#)]
10. Afroze, S.; Reza, M.S.; Cheok, Q.; Islam, S.N.; Abdalla, A.M.; Taweekun, J.; Azad, A.K.; Khalilpoor, N.; Issakhov, A. Advanced applications of fuel cells during the COVID-19 Pandemic. *Int. J. Chem. Eng.* **2021**, *2021*, 5539048. [[CrossRef](#)]
11. Dincer, I. Renewable energy and sustainable development: A crucial review. *Renew. Sustain. Energy Rev.* **2000**, *4*, 157–175. [[CrossRef](#)]
12. Stambouli, A.B.; Traversa, E. Solid oxide fuel cells (SOFCs): A review of an environmentally clean and efficient source of energy. *Renew. Sustain. Energy Rev.* **2002**, *6*, 433–455. [[CrossRef](#)]
13. Panwar, N.L.; Kaushik, S.C.; Kothari, S. Role of renewable energy sources in environmental protection: A review. *Renew. Sustain. Energy Rev.* **2011**, *15*, 1513–1524. [[CrossRef](#)]
14. Dincer, I.; Rosen, M.A. Sustainability aspects of hydrogen and fuel cell systems. *Int. J. Sustain. Energy Dev.* **2011**, *15*, 137–146. [[CrossRef](#)]
15. Branco, H.; Castro, R.; Lopes, A.S. Battery energy storage systems as a way to integrate renewable energy in small isolated power systems. *Int. J. Sustain. Energy Dev.* **2018**, *43*, 90–99. [[CrossRef](#)]
16. International Energy Agency. The Future of Hydrogen: Seizing today’s opportunities. *OECD* **2019**. [[CrossRef](#)]
17. Abe, J.O.; Popoola, A.P.I.; Ajenifuja, E.; Popoola, O.M. Hydrogen energy, economy and storage: Review and recommendation. *Int. J. Hydrog. Energy* **2019**, *44*, 15072–15086. [[CrossRef](#)]

18. Dawood, F.; Anda, M.; Shafiullah, G.M. Hydrogen production for energy: An overview. *Int. J. Hydrog. Energy* **2019**, *45*, 3847–3869. [[CrossRef](#)]
19. Easily, R.R.; Chi, Y.; Ibrahim, D.M.; Chen, Y. Hydrogen strategy in decarbonization era: Egypt as a case study. *Int. J. Hydrog. Energy* **2022**, *47*, 18629–18647. [[CrossRef](#)]
20. Arsad, A.Z.; Hannan, M.A.; Al-Shetwi, A.Q.; Mansur, M.; Muttaqi, K.M.; Dong, Z.Y.; Blaabjerg, F. Hydrogen energy storage integrated hybrid renewable energy systems: A review analysis for future research directions. *Int. J. Hydrog. Energy* **2022**, *47*, 17285–17312. [[CrossRef](#)]
21. Scovell, M.D. Explaining hydrogen energy technology acceptance: A critical review. *Int. J. Hydrog. Energy* **2022**, *47*, 10441–10459. [[CrossRef](#)]
22. Abdalla, A.M.; Hossain, S.; Nisfindy, O.B.; Azad, A.T.; Dawood, M.; Azad, A.K. Hydrogen production, storage, transportation and key challenges with applications: A review. *Energy Convers. Manag.* **2018**, *165*, 602–627. [[CrossRef](#)]
23. Hossain, S.; Abdalla, A.M.; Jamain, S.N.B.; Zaini, J.H.; Azad, A.K. A review on proton conducting electrolytes for clean energy and intermediate temperature-solid oxide fuel cells. *Renew. Sustain. Energy Rev.* **2017**, *79*, 750–764. [[CrossRef](#)]
24. Kim, J.; Sengodan, S.; Kim, S.; Kwon, O.; Bu, Y.; Kim, G. Proton conducting oxides: A review of materials and applications for renewable energy conversion and storage. *Renew. Sustain. Energy Rev.* **2019**, *109*, 606–618. [[CrossRef](#)]
25. Zhang, W.; Hu, Y.H. Progress in proton-conducting oxides as electrolytes for low-temperature solid oxide fuel cells: From materials to devices. *Energy Sci. Eng.* **2021**, *9*, 984–1011. [[CrossRef](#)]
26. Meng, Y.; Gao, J.; Zhao, Z.; Amoroso, J.; Tong, J.; Brinkman, K.S. Review: Recent progress in low-temperature proton-conducting ceramics. *J. Mater. Sci.* **2019**, *54*, 9291–9312. [[CrossRef](#)]
27. Medvedev, D. Trends in research and development of protonic ceramic electrolysis cells. *Int. J. Hydrog. Energy* **2019**, *44*, 26711–26740. [[CrossRef](#)]
28. Medvedev, D.A. Current drawbacks of proton-conducting ceramic materials: How to overcome them for real electrochemical purposes. *Curr. Opin. Green Sustain. Chem.* **2021**, *32*, 100549. [[CrossRef](#)]
29. Zvonareva, I.; Fu, X.-Z.; Medvedev, D.; Shao, Z. Electrochemistry and energy conversion features of protonic ceramic cells with mixed ionic-electronic electrolytes. *Energy Environ. Sci.* **2022**, *15*, 439–465. [[CrossRef](#)]
30. Shim, J.H. Ceramics breakthrough. *Nature Energy* **2018**, *3*, 168–169. [[CrossRef](#)]
31. Bello, I.T.; Zhai, S.; He, Q.; Cheng, C.; Dai, Y.; Chen, B.; Zhang, Y.; Ni, M. Materials development and prospective for protonic ceramic fuel cells. *Int. J. Energy Res.* **2021**, *46*, 2212–2240. [[CrossRef](#)]
32. Chiara, A.; Giannici, F.; Pipitone, C.; Longo, A.; Aliotta, C.; Gambino, M.; Martorana, A. Solid-Solid Interfaces in Protonic Ceramic Devices: A Critical Review. *ACS Appl. Mater. Interfaces* **2020**, *12*, 55537–55553. [[CrossRef](#)] [[PubMed](#)]
33. Cao, J.; Ji, Y.; Shao, Z. New Insights into the Proton-Conducting Solid Oxide Fuel Cells. *J. Chin. Ceram. Soc.* **2021**, *49*, 83–92. [[CrossRef](#)]
34. Bello, I.T.; Zhai, S.; Zhao, S.; Li, Z.; Yu, N.; Ni, M. Scientometric review of proton-conducting solid oxide fuel cells. *Int. J. Hydrog. Energy* **2021**, *46*, 37406–37428. [[CrossRef](#)]
35. Colomban, P. Proton conductors and their applications: A tentative historical overview of the early researches. *Solid State Ionics* **2019**, *334*, 125–144. [[CrossRef](#)]
36. Iwahara, H.; Esaka, T.; Uchida, H.; Maeda, N. Proton conduction in sintered oxides and its application to steam electrolysis for hydrogen production. *Solid State Ion.* **1981**, *3–4*, 359–363. [[CrossRef](#)]
37. Iwahara, H.; Uchida, H.; Maeda, N. High temperature fuel and steam electrolysis cells using proton conductive solid electrolytes. *J. Power Sources* **1982**, *7*, 293–301. [[CrossRef](#)]
38. Iwahara, H.; Uchida, H.; Tanaka, S. High temperature type proton conductors based on SrCeO₃ and its application to solid electrolyte fuel cells. *Solid State Ion.* **1983**, *9–10*, 1021–1025. [[CrossRef](#)]
39. Irvine, J.; Rupp, J.L.M.; Liu, G.; Xu, X.; Haile, S.; Qian, X.; Snyder, A.; Freer, R.; Ekren, D.; Skinner, S.; et al. Roadmap on inorganic perovskites for energy applications. *J. Phys. Energy* **2021**, *3*, 031502. [[CrossRef](#)]
40. Hossain, M.K.; Chanda, R.; El-Denglawey, A.; Emrose, T.; Rahman, M.T.; Biswas, M.C.; Hashizume, K. Recent progress in barium zirconate proton conductors for electrochemical hydrogen device applications: A review. *Ceram. Int.* **2021**, *47*, 23725–23748. [[CrossRef](#)]
41. Tarasova, N.; Colomban, P.; Animitsa, I. The short-range structure and hydration process of fluorine-substituted double perovskites based on barium-calcium niobate Ba₂CaNbO_{5.5}. *J. Phys. Chem. Solids* **2018**, *118*, 32–39. [[CrossRef](#)]
42. Cichy, K.; Skubida, W.; Świerczek, K. Structural transformations, water incorporation and transport properties of tin-substituted barium indate. *J. Solid State Chem.* **2018**, *262*, 58–67. [[CrossRef](#)]
43. Domen, K.; Yoshimura, J.; Sekine, T.; Tanaka, A.; Onishi, T. A novel series of photocatalysts with an ion-exchangeable layered structure of niobate. *Catal Lett.* **1990**, *4*, 339–343. [[CrossRef](#)]
44. Machida, M.; Yabunaka, J.; Kijima, T. Efficient photocatalytic decomposition of water with the novel layered tantalate RbNdTa₂O₇. *Chem. Commun.* **1999**, *19*, 1939–1940. [[CrossRef](#)]
45. Machida, M.; Miyazaki, K.; Matsushima, S.; Arai, M. Photocatalytic properties of layered perovskite tantalates, MLnTa₂O₇ (M = Cs, Rb, Na, and H; Ln = La, Pr, Nd, and Sm). *J. Mater. Chem.* **2003**, *13*, 1433–1437. [[CrossRef](#)]
46. Rodionov, I.A.; Zvereva, I.A. Photocatalytic activity of layered perovskite-like oxides in practically valuable chemical reactions. *Russ. Chem. Rev.* **2016**, *85*, 248–279. [[CrossRef](#)]

47. Krashenninnikova, O.V.; Syrov, E.V.; Smirnov, S.M.; Suleimanov, E.V.; Fukina, D.G.; Knyazev, A.V.; Titaev, D.N. Synthesis, crystal structure and photocatalytic activity of new Dion-Jacobson type titanoniobates. *J. Solid State Chem.* **2022**, *315*, 123445. [[CrossRef](#)]
48. Phuruangrat, A.; Ekthammathat, N.; Dumrongrojanath, P.; Thingtem, S.; Thongtem, T. Hydrothermal synthesis, structure, and optical properties of pure and silver-doped Bi₂MoO₆ nanoplates. *Russ. J. Phys. Chem.* **2015**, *89*, 2443–2448. [[CrossRef](#)]
49. Chawla, H.; Chandra, A.; Ingole, P.P.; Garg, S. Recent advancements in enhancement of photocatalytic activity using bismuth-based metal oxides Bi₂MO₆ (M = W, Mo, Cr) for environmental remediation and clean energy production. *Ind. Eng. Chem. Res.* **2021**, *95*, 1–15. [[CrossRef](#)]
50. Tasleem, S.; Tahir, M. Recent progress in structural development and band engineering of perovskites materials for photocatalytic solar hydrogen production: A review. *Int. J. Hydrog. Energy* **2020**, *45*, 19078–19111. [[CrossRef](#)]
51. Huang, Y.; Liu, J.; Deng, Y.; Qian, Y.; Jia, X.; Ma, M.; Yang, C.; Liu, K.; Wang, Z.; Qu, S.; et al. The application of perovskite materials in solar water splitting. *J. Semicond.* **2020**, *41*, 011701. [[CrossRef](#)]
52. Zhang, G.; Liu, G.; Wang, L.; Irvine, J.T.S. Inorganic perovskite photocatalysts for solar energy utilization. *Chem. Soc. Rev.* **2016**, *45*, 5951–5984. [[CrossRef](#)] [[PubMed](#)]
53. Zhang, P.; Zhang, J.; Gong, J. Tantalum-based semiconductors for solar water splitting. *Chem. Soc. Rev.* **2014**, *43*, 4395–4422. [[CrossRef](#)] [[PubMed](#)]
54. Benedek, N.A.; Rondinelli, J.M.; Djani, H.; Ghosez, P.; Lightfoot, P. Understanding ferroelectricity in layered perovskites: New ideas and insights from theory and experiments. *Dalton Trans.* **2015**, *44*, 10543–10558. [[CrossRef](#)]
55. Ferreira, W.C.; Rodrigues, G.L.C.; Araújo, B.S.; de Aguiar, F.A.A.; de Abreu Silva, A.N.A.; Fechine, P.B.A.; de Araujo Paschoal, C.W.; Ayala, A.P. Pressure-induced structural phase transitions in the multiferroic four-layer Aurivillius ceramic Bi₅FeTi₃O₁₅. *Ceramics* **2020**, *46*, 18056–180621. [[CrossRef](#)]
56. Zuhadri, W.; Wondari, T.P.; Ikram, M.; Putri, Y.E.; Septiani, U.; Imelda. Enhanced dielectric and ferroelectric responses in La³⁺/Ti⁴⁺ co-substituted SrBi₂Ta₂O₉ Aurivillius phase. *Ceram. Int.* **2022**, *48*, 10328–103321. [[CrossRef](#)]
57. Xu, Q.; Xie, S.; Wang, F.; Liu, J.; Shi, J.; Xing, J.; Chen, Q.; Zhu, J.; Wang, Q. Bismuth titanate based piezoceramics: Structural evolutions and electrical behaviors at different sintering temperatures. *J. Alloys Compd.* **2021**, *882*, 160637. [[CrossRef](#)]
58. Chen, C.; Ning, H.; Lepadatu, S.; Cain, M.; Yan, H.; Reece, M.J. Ferroelectricity in Dion-Jacobson ABiNb₂O₇ (A = Rb, Cs) compounds. *J. Mater. Chem. C* **2015**, *3*, 19–22. [[CrossRef](#)]
59. Kudo, A.; Kaneko, E. Photoluminescence of layered perovskite oxides with triple-octahedra slabs containing titanium and niobium. *J. Mater. Sci. Lett.* **1997**, *16*, 224–226. [[CrossRef](#)]
60. Pavani, K.; Graça, M.P.F.; Kumar, J.S.; Neves, A.J. Photoluminescence varied by selective excitation in BiGdWO₆:Eu³⁺ phosphor. *Opt. Mater.* **2017**, *74*, 120–127. [[CrossRef](#)]
61. Mamidi, S.; Gundeboina, R.; Kurra, S.; Velchuri, R.; Muga, V. Aurivillius family of layered perovskites, BiREWO₆ (RE = La, Pr, Gd, and Dy): Synthesis, characterization, and photocatalytic studies. *C. R. Chim.* **2018**, *21*, 547–552. [[CrossRef](#)]
62. Zhou, G.; Jiang, X.; Zhao, J.; Molokeev, M.; Lin, Z.; Liu, Q.; Xia, Z. Two-dimensional-layered perovskite ALaTa₂O₇:Bi³⁺ (A = K and Na) phosphors with versatile structures and tunable photoluminescence. *ACS Appl. Mater. Interfaces* **2018**, *10*, 24648–24655. [[CrossRef](#)] [[PubMed](#)]
63. Panda, D.P.; Singh, A.K.; Kundu, T.K.; Sundaresan, A. Visible-light excited polar Dion-Jacobson Rb(Bi_{1-x}Eu_x)₂Ti₂NbO₁₀ perovskites: Photoluminescence properties and in vitro bioimaging. *J. Mater. Chem. B* **2022**, *10*, 935–944. [[CrossRef](#)]
64. Ruddlesden, S.N.; Popper, P. New compounds of the K₂NiF₄ type. *Acta Cryst.* **1957**, *10*, 538–539. [[CrossRef](#)]
65. Ruddlesden, S.N.; Popper, P. The compound Sr₃Ti₂O₇ and its structure. *Acta Cryst.* **1958**, *11*, 54–55. [[CrossRef](#)]
66. Ganguly, P.; Rao, C.N.R. Crystal Chemistry and Magnetic Properties of Layered Metal Oxides Possessing the K₂NiF₄ or Related Structures. *J. Solid State Chem.* **1984**, *53*, 193–216. [[CrossRef](#)]
67. Ganculi, D. Cationic radius ratio and formation of K₂NiF₄-type compounds. *J. Solid State Chem.* **1979**, *30*, 353–356. [[CrossRef](#)]
68. Tyitov, Y.O.; Slobodyanik, M.S.; Polubinskii, V.V. Criteria of existence of one- and two-layer compounds (Me^{II}Ln)_{n+1}B_nO_{3n+1}. *Dopov. Natsyional'noyi Akad. Nauk. Ukrayini* **2018**, *2018*, 80–85. [[CrossRef](#)]
69. Tyitov, Y.O.; Byilyavina, N.M.; Markyiv, V.Y.; Slobodyanik, M.S.; Krajevs'ka, Y.A. Synthesis and crystal structure of BaLaInO₄ and SrLnInO₄ (Ln—La, Pr). *Dopov. Natsyional'noyi Akad. Nauk. Ukrayini* **2009**, *10*, 160–166.
70. Fijii, K.; Yashima, M. Discovery and development of BaNdInO₄ -A brief review. *J. Ceram. Soc. Jpn.* **2018**, *126*, 852–859. [[CrossRef](#)]
71. Chroneos, A.; Yildiz, B.; Tarancón, A.; Parfitt, D.; Kilner, J.A. Oxygen diffusion in solid oxide fuel cell cathode and electrolyte materials: Mechanistic insights from atomistic simulations. *Energy Environ. Sci.* **2011**, *4*, 2774–2789. [[CrossRef](#)]
72. Yang, X.; Liu, S.; Lu, F.; Xu, J.; Kuang, X. Acceptor Doping and Oxygen Vacancy Migration in Layered Perovskite NdBaInO₄-Based Mixed Conductors. *J. Phys. Chem. C* **2016**, *120*, 6416–6426. [[CrossRef](#)]
73. Fujii, K.; Esaki, Y.; Omoto, K.; Yashima, M.; Hoshikawa, A.; Ishigaki, T.; Hester, J.R. New Perovskite-Related Structure Family of Oxide-Ion Conducting Materials NdBaInO₄. *Chem. Mater.* **2014**, *26*, 2488–2491. [[CrossRef](#)]
74. Tarasova, N.; Galisheva, A.; Animitsa, I.; Korona, D.; Kreimesh, H.; Fedorova, I. Protonic transport in layered perovskites BaLa_nIn_nO_{3n+1} (n = 1, 2) with Ruddlesden-Popper structure. *Appl. Sci.* **2022**, *12*, 4082. [[CrossRef](#)]
75. Tarasova, N.; Galisheva, A.; Animitsa, I.; Belova, K.; Egorova, A.; Abakumova, E.; Medvedev, D. Layered Perovskites BaM₂In₂O₇ (M = La, Nd): From the Structure to the Ionic (O²⁻, H⁺) Conductivity. *Materials* **2022**, *15*, 3488. [[CrossRef](#)]
76. Tarasova, N.; Animitsa, I.; Galisheva, A. Electrical properties of new protonic conductors Ba_{1+x}La_{1-x}InO_{4-0.5x} with Ruddlesden-Popper structure. *J. Solid State Electrochem.* **2020**, *24*, 1497–1508. [[CrossRef](#)]

77. Tarasova, N.; Animitsa, I.; Galisheva, A. Effect of acceptor and donor doping on the state of protons in block-layered structures based on BaLaInO₄. *Solid State Comm.* **2021**, *323*, 114093. [[CrossRef](#)]
78. Tarasova, N.; Galisheva, A.; Animitsa, I. Improvement of oxygen-ionic and protonic conductivity of BaLaInO₄ through Ti doping. *Ionics* **2020**, *26*, 5075–5088. [[CrossRef](#)]
79. Tarasova, N.A.; Galisheva, A.O.; Animitsa, I.E.; Lebedeva, E.L. Oxygen-Ion and Proton Transport in Sc-Doped Layered Perovskite BaLaInO₄. *Russ. J. Electrochem.* **2021**, *57*, 1008–1014. [[CrossRef](#)]
80. Tarasova, N.; Galisheva, A.; Animitsa, I.; Anokhina, I.; Gilev, A.; Cheremisina, P. Novel mid-temperature Y³⁺ → In³⁺ doped proton conductors based on the layered perovskite BaLaInO₄. *Ceram. Int.* **2022**, *48*, 15677–15685. [[CrossRef](#)]
81. Tarasova, N.; Bedarkova, A.; Animitsa, I. Proton transport in the gadolinium-doped layered perovskite BaLaInO₄. *Materials* **2022**, *15*, 7351. [[CrossRef](#)] [[PubMed](#)]
82. Tarasova, N.; Bedarkova, A. Advanced proton-conducting ceramics based on layered perovskite BaLaInO₄ for energy conversion technologies and devices. *Materials* **2022**, *15*, 6841. [[CrossRef](#)] [[PubMed](#)]
83. Tarasova, N.; Animitsa, I.; Galisheva, A.; Korona, D. Incorporation and Conduction of Protons in Ca, Sr, Ba-Doped BaLaInO₄ with Ruddlesden-Popper Structure. *Materials* **2019**, *12*, 1668. [[CrossRef](#)] [[PubMed](#)]
84. Fujii, K.; Shiraiwa, M.; Esaki, Y.; Yashima, M.; Kim, S.J.; Lee, S. Improved oxide-ion conductivity of NdBaInO₄ by Sr doping. *J. Mater. Chem. A* **2015**, *3*, 11985–11990. [[CrossRef](#)]
85. Ishihara, T.; Yan, Y.; Sakai, T.; Ida, S. Oxide ion conductivity in doped NdBaInO₄. *Solid State Ion.* **2016**, *288*, 262–265. [[CrossRef](#)]
86. Zhou, Y.; Shiraiwa, M.; Nagao, M.; Fujii, K.; Tanaka, I.; Yashima, M.; Bague, L.; Basbus, J.F.; Moggi, L.V.; Skinner, S.J. Protonic conduction in the BaNdInO₄ structure achieved by acceptor doping. *Chem. Mater.* **2021**, *33*, 2139–2146. [[CrossRef](#)]
87. Proton Transport in Alkali-Earth Doped Layered Perovskites Based on BaLa₂In₂O₇. *Inorganics* **2022**, *10*, 161. [[CrossRef](#)]
88. Tarasova, N.A. Local structure and ionic transport in acceptor-doped layered perovskite BaLa₂In₂O₇. *Chim. Techno Acta* **2022**, *9*, 20229415. [[CrossRef](#)]
89. Tarasova, N.; Bedarkova, A.; Animitsa, I.; Abakumova, E.; Belova, K.; Kreimesh, H. Novel high conductive ceramic materials based on two-layer perovskite BaLa₂In₂O₇. *Int. J. Mol. Sci.* **2022**, *23*, 12813. [[CrossRef](#)]
90. Tarasova, N.; Bedarkova, A.; Animitsa, I.; Verinkina, E. Synthesis, Hydration Processes and Ionic Conductivity of Novel Gadolinium-Doped Ceramic Materials Based on Layered Perovskite BaLa₂In₂O₇ for Electrochemical Purposes. *Processes* **2022**, *10*, 2536. [[CrossRef](#)]
91. Tarasova, N.; Bedarkova, A.; Animitsa, I.; Abakumova, E. Cation and oxyanion doping of layered perovskite BaNd₂In₂O₇: Oxygen-ion and proton transport. *Int. J. Hydrog. Energy* **2022**, *in press*. [[CrossRef](#)]

Disclaimer/Publisher's Note: The statements, opinions and data contained in all publications are solely those of the individual author(s) and contributor(s) and not of MDPI and/or the editor(s). MDPI and/or the editor(s) disclaim responsibility for any injury to people or property resulting from any ideas, methods, instructions or products referred to in the content.